ADVANCED ENERGY MATERIALS

Supporting Information

for *Adv. Energy Mater.*, DOI 10.1002/aenm.202302288

Interface Coating Design for Dynamic Voltage Stability of Solid-State Batteries

*Yichao Wang, Luhan Ye, William Fitzhugh, Xi Chen and Xin Li**

Supplementary information

Interface coating design for dynamic voltage stability of solid state batteries

Table S1. Summary of the ionic conductivity and computation results of the electrolytes.

Electrolyte	σ_{ionic} (mS/cm)	$\log \sigma_{ionic}$	R_w	k_{ox}	k_{re}	k_{ox} - k_{re}	intrinsic window	reference
$Li_{10}Ge(PS_6)_2$	12	-1.92	0.19	0.09	-0.06	0.15	0.80	[1]
$Li_{10}Sn(PS_6)_2$	4	-2.40	0.14	0.08	-0.02	0.10	0.70	[2]
$Li_7P_3S_{11}$	17	-1.77	0.26	0.09	-0.07	0.16	0.60	[3]
$Li_{10}Si(PS_6)_2$	23	-1.64	0.14	0.08	-0.05	0.13	0.90	[4]
$Li_{20}Si_3P_3S_{23}Cl$	25	-1.60	0.15	0.07	-0.05	0.12	0.80	[5]
Li_3PS_4	0.16	-3.80	0.18	0.08	-0.06	0.14	0.80	[6]
$Li_{5.5}PS_{4.5}Cl_{1.5}$	12	-1.92	0.20	0.10	-0.07	0.16	0.80	[7]
Li_3YCl_6	0.5	-3.30	0.09	0.18	-0.13	0.31	3.60	[8]
Li_3YBr_6	1.7	-2.77	0.10	0.12	-0.15	0.27	2.60	[8]
Li_3ErCl_6	0.3	-3.52	0.10	0.20	-0.16	0.36	3.40	[9]
Li_3InCl_6	1.49	-2.83	0.14	0.17	-0.12	0.29	2.10	[10]
Li_3ScCl_6	3	-2.52	0.08	0.16	-0.13	0.29	3.50	[11]
$Li_{1.3}Al_{0.3}Ti_{1.7}(PO_4)_3$	0.7	-3.15	0.10	0.14	-0.10	0.24	2.30	[12]
$Li_{0.5}La_{0.5}TiO_3$	1.08	-3.24	0.03	0.08	0.00	0.08	2.50	[13]
$Li_7La_3Zr_2O_{12}$	0.5	-3.30	0.06	0.07	-0.10	0.17	3.00	[14]
Li_3OCl	0.85	-3.07	0.03	0.10	0.00	0.10	2.80	[15]

Table S2. LGPS 4V stability

LGPS 4V stability (Reference Volume = V_{LGPS})			
K_{eff} (GPa)	decomposition energy (eV/atom)	strain	Decomposition products
0	0.988	0.302	10 Li + 3 S + P2S7 + 1 GeS2
10	0.183	0.264	8.8 Li + 2.4 S1 + P2S7 + 0.7 Ge1S2 + 0.3 Li4Ge1S4
20	0.000	0.000	Li10Ge1P2S12

As shown in Table S2, without mechanical constriction, LGPS decomposition leads to 30.2% reaction strain with 0.988 eV/atom decomposition energy. When we assign $K_{eff}\varepsilon V_{LGPS}$ energy penalty to each reaction with different reaction strain ε, the sequence of the decomposition energy magnitude in the reaction space changes. Reactions with larger ε will have larger $K_{eff}\varepsilon V_{LGPS}$ penalty, thus increasing K_{eff} will make reactions with smaller ε have larger decomposition energy in the reaction space, leading to a change of ground state reaction toward smaller ε with increasing K_{eff}. At K_{eff} = 20 GPa, LGPS does not decompose, suggesting a critical K_{eff} (i.e., K_{crit} or K*) between 10 GPa and 20 GPa, beyond which there is no oxidative decomposition reaction for LGPS.

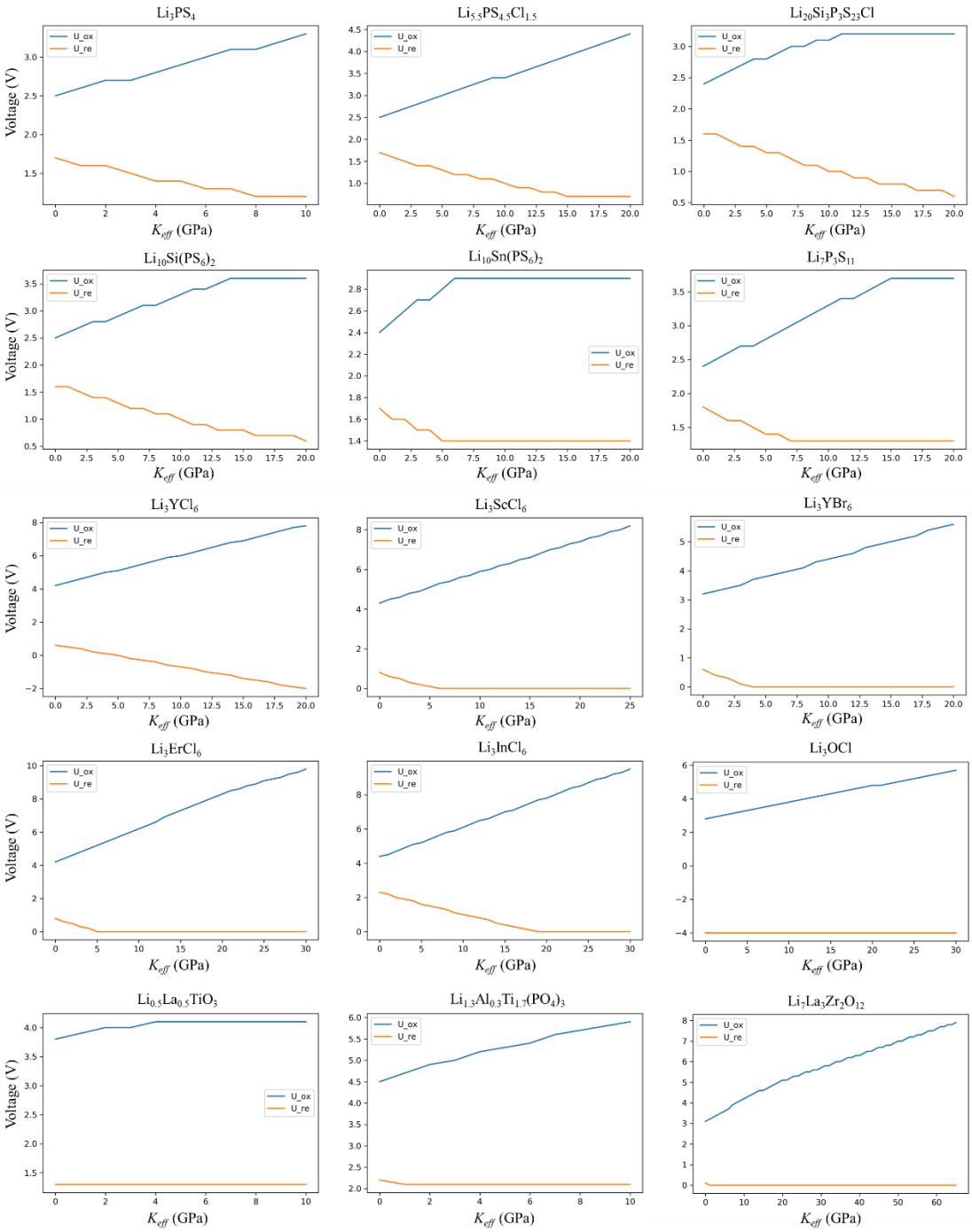

Figure S1. Voltage stability window in response to mechanical constriction for different electrolytes.

Technically, when K_{eff} is small, perturbation method (see Methods) is approximately equal to minimization method. We know that in perturbation method, only the decomposition reaction with the highest reaction energy at 0 GPa is considered, so we take the derivative of equation (5) in Methods with respect to the K_{eff} for both oxidation reaction and reduction reaction:

$$U'\left(K_{eff}\right)_{ox} = \frac{V_{SSE}\varepsilon_{ox}}{n_{ox}e} = k_{ox} \tag{1}$$

$$U'(K_{eff})_{re} = \frac{V_{SSE}\varepsilon_{re}}{n_{re}e} = k_{re} \quad (2)$$

Equations. (1) and (2) show that the volume of the electrolyte, the reaction strain, and the number of charge (or Lithium) transferred together decide the k_{ox} and k_{re}. For example, comparing the k_{ox} between Li_3YCl_6 and LGPS, Li_3YCl_6 shows 13% larger atomic volume, 28% larger reaction strain and 33% larger $1/n_{ox}$ that in the end gives 92% larger k_{ox}, which is very close to the 100% larger k_{ox} calculated by the minimization method (Fig. 2d, Table S1).

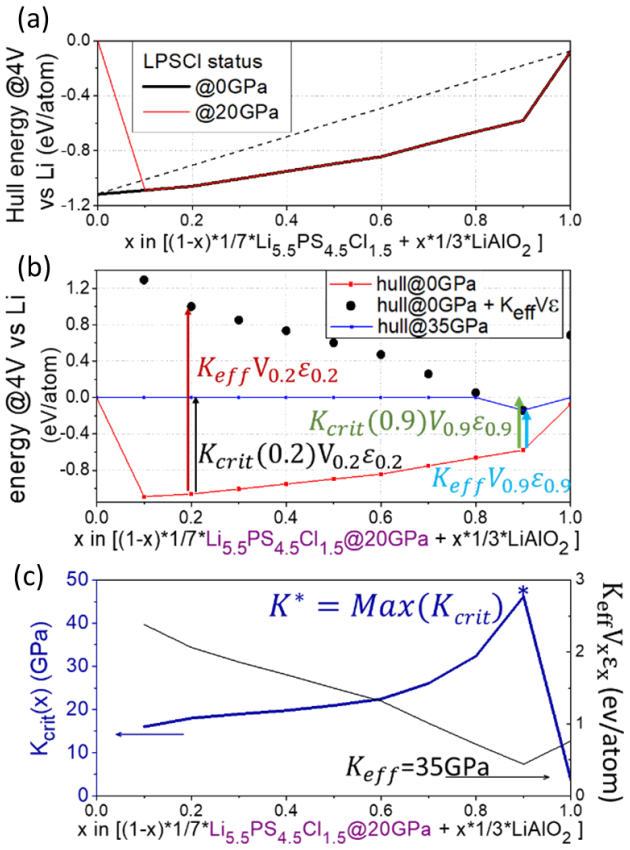

Figure S2. (a) Comparison of hull energies at 4 V versus Li of $\{Li_{5.5}PS_{4.5}Cl_{1.5}$-$LiAlO_2\}$ interface with unconstructed $Li_{5.5}PS_{4.5}Cl_{1.5}$ and constricted $Li_{5.5}PS_{4.5}Cl_{1.5}$ at K_{eff} = 20 GPa ($Li_{5.5}PS_{4.5}Cl_{1.5}$@20GPa). The dashed line corresponds to the sum of intrinsic instability of $Li_{5.5}PS_{4.5}Cl_{1.5}$and $LiAlO_2$ at 4V. (b) Illustration of the change of hull after applying 35 GPa mechanical constriction at the interface of $\{Li_{5.5}PS_{4.5}Cl_{1.5}$@20GPa-$LiAlO_2\}$ at 4 V, and the comparison between $K_{crit}(x)V_x\varepsilon_x$ and $K_{eff}V_x\varepsilon_x$. (c) $K_{eff}V_x\varepsilon_x$ of $\{Li_{5.5}PS_{4.5}Cl_{1.5}$@20GPa-$LiAlO_2\}$ interface at 4V at K_{eff} = 35 GPa, and the definition of K^*.

In calculating the stability of interface and the effect of mechanical constriction, the pseudo-phase method[16] is adopted to interpolate the phase energy, composition and volume of two phases. The solid black curve in Figure S2a is an example of using the pseudo-phase method to calculate the interface hull of $Li_{5.5}PS_{4.5}Cl_{1.5}$ and $LiAlO_2$. The dashed line interpolates the hull of $Li_{5.5}PS_{4.5}Cl_{1.5}$ and $LiAlO_2$, showing the part of instability of the interface contributed by the intrinsic instability of the two ends. If the hull is below the dashed line, there is interfacial

reaction between the two ends, which is the case of the {$Li_{5.5}PS_{4.5}Cl_{1.5}$-$LiAlO_2$} interface shown here. The interface hull is defined as the most negative hull among all the composition x in the solid black curve. But due to large decomposition energy of sulfide electrolyte, the interface hull will be the hull of sulfide electrolyte itself in most cases, which does not reveal the meaningful information of the interface, therefore we apply certain K_{eff} (20 GPa here) to stabilize the electrolyte by raising the $Li_{5.5}PS_{4.5}Cl_{1.5}$ decomposition reaction energy to be positive and keeping the energy of $Li_{5.5}PS_{4.5}Cl_{1.5}$ itself unchanged, so the difference between the hull curve of {$Li_{5.5}PS_{4.5}Cl_{1.5}$-$LiAlO_2$} and {$Li_{5.5}PS_{4.5}Cl_{1.5}$@20GPa-$LiAlO_2$} is the difference in hull at the end point of $Li_{5.5}PS_{4.5}Cl_{1.5}$. From x = 0 to x = 0.1, the metastability of the $Li_{5.5}PS_{4.5}Cl_{1.5}$ is perturbed by the interfacial reaction, thus the large decomposition energy. The interface hull then shifts from that of the $Li_{5.5}PS_{4.5}Cl_{1.5}$ end point to that of x = 0.1.

Treating pseudo phase at each composition x (*pp(x)*) as a solid-state electrolyte and using $\Delta G_{EC-RXN} = G_{Dec} + n(G_{Li} - eU) - G_{SSE} + K_{eff}V_{SSE}\varepsilon$ (eqn. 2 in Methods), we can evaluate the constriction induced voltage stability of the interface. Each *pp(x)* has its own G_{Dec}, $n, G_{pp(x)}, V_x$ and ε_x. Fig. S2b shows how 35 GPa mechanical constriction affects the hull of {$Li_{5.5}PS_{4.5}Cl_{1.5}$@20GPa-$LiAlO_2$} interface. For example, at x = 0.2, when being normalized to 1 closed atom per formula, the volume V(1/7 $Li_{5.5}PS_{4.5}Cl_{1.5}$) = 128.78 Å^3/closed atom, and the volume V(1/3 $LiAlO_2$) = 13.806 Å^3/closed atom, thus at x = 0.2, the pseudo phase volume $V_{0.2}$ = 0.2* V(1/3 $LiAlO_2$) + 0.8* V(1/7 $Li_{5.5}PS_{4.5}Cl_{1.5}$) = 0.2*13.806 + 0.8*128.78 = 105.79 Å^3/closed atom. $K_{eff}V_{0.2}\varepsilon_{0.2}$ well exceeds the hull and brings the decomposition reaction energy to ~ +1eV as shown by the long red arrow, so that the decomposition is suppressed and the hull at x = 0.2 becomes 0 by definition. At x = 0.9, however, the $K_{eff}V_{0.2}\varepsilon_{0.2}$ is not large enough to bring the decomposition energy to be positive, thus the interface can still decompose at K_{eff} = 35 GPa, but the decomposition energy is much smaller, suggesting a more stable {$Li_{5.5}PS_{4.5}Cl_{1.5}$-$LiAlO_2$} interface. We define $K_{crit}(x)$ to demonstrate the level of mechanical constriction just needed to suppress decomposition reaction of *pp(x)* as shown in Fig S2b by the thick green arrow at x = 0.9 and the black arrow at x = 0.2, which is the K_{eff} value to equate eqn. (8) in the main text to 0, and gives eqn. (9).

That is to say, at composition x, the particular decomposition reaction is suppressed if and only if $K_{eff} > K_{crit_x}$. As K_{crit} is a function of x, therefore, to suppress the reaction between two phases, the largest $K_{crit}(x)$ has to be reached. We define the largest $K_{crit}(x)$ to be K^* (eqn. 10). Fig. S2c shows the K_{crit} of {$Li_{5.5}PS_{4.5}Cl_{1.5}$-$LiAlO_2$} interface at 4V and labels the K^*. The $K_{eff}V_x\varepsilon_x$ is also plotted in Fig. S2c and shows a minimum at x = 0.9, coinciding the x for maximum K_{crit_x}. From Fig. S2a, the absolute value of hull at x = 0.9 is actually the smallest among the hull from x = 0.1 to x = 0.9, but due to its smallest $V_x\varepsilon_x$ (or smallest $K_{eff}V_x\varepsilon_x$), the $K_{crit}(0.9)$ becomes the largest $K_{crit}(x)$, suggesting that the smallest mechanical response is at x = 0.9.

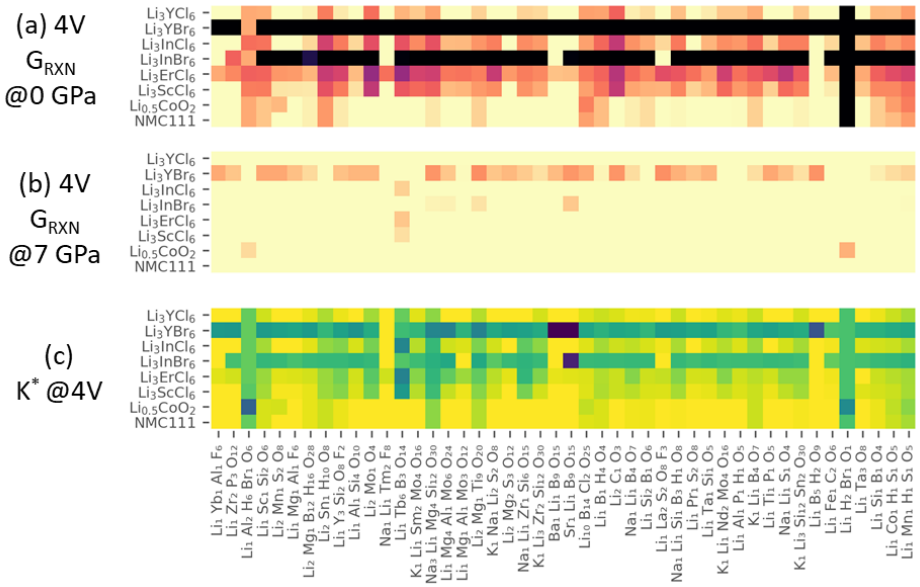

Figure S3. Halide electrolyte / oxide cathode coating after including Li_xCl_y as possible decomposition products.

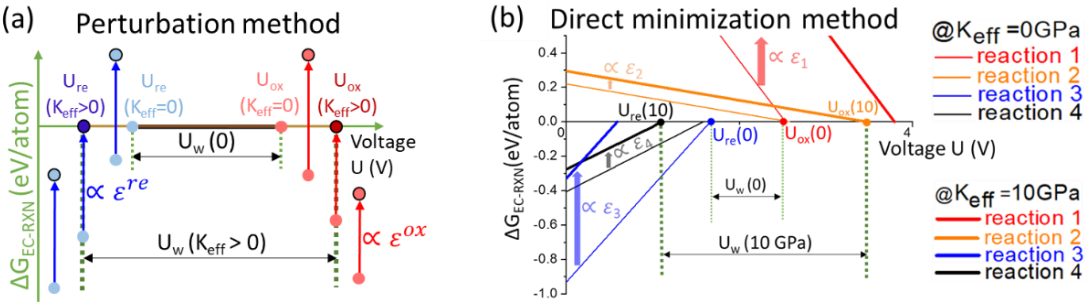

Figure S4. Constriction induced voltage stability of the decomposition reaction of solid-state electrolyte (SSE). ΔG_{EC-RXN} is the Gibbs free energy of the electrochemical decomposition reaction. U_{re} (K_{eff}), U_{ox} (K_{eff}) and U_w (K_{eff}) are the reduction limit, oxidation limit and the voltage stability window of the electrolyte, respectively, which are all functions of the effective modulus K_{eff} in the unit of GPa representing the local level of mechanical constriction. ε is the reaction strain of a specific decomposition. (a) Perturbation method with just one oxidative decomposition reaction (red dots) and one reductive decomposition reaction (blue dots) at each voltage. The upward arrows show that the electrochemical decomposition energy is increased by mechanical constriction and the magnitude is proportional to reaction strain; (b) Direct minimization method demonstrated by an example of $Li_{10}GeP_2S_{12}$ (LGPS): all decomposition reactions are considered and the 4 voltage window determining reactions in the illustration are labeled with 4 different colors. The 4 thin solid lines show the electrochemical reaction Gibbs free energy change with respect to voltage without mechanical constriction, and the 4 solid thick lines show that of the reactions with effective modulus K_{eff} of 10 GPa.

Reference

1. Kamaya, N.; Homma, K.; Yamakawa, Y.; Hirayama, M.; Kanno, R.; Yonemura, M.; Kamiyama, T.; Kato, Y.; Hama, S.; Kawamoto, K., A lithium superionic conductor. *Nat. Mater.* **2011,** *10* (9), 682-686.
2. Bron, P.; Johansson, S.; Zick, K.; Schmedt auf der Günne, J. r.; Dehnen, S.; Roling, B., Li10SnP2S12: an affordable lithium superionic conductor. *J. Am. Chem. Soc.* **2013,** *135* (42), 15694-15697.
3. Seino, Y.; Ota, T.; Takada, K.; Hayashi, A.; Tatsumisago, M., A sulphide lithium super ion conductor is superior to liquid ion conductors for use in rechargeable batteries. *Energy Environ. Sci.* **2014,** *7* (2), 627-631.
4. Zhang, B.; Yang, L.; Wang, L.-W.; Pan, F., Cooperative transport enabling fast Li-ion diffusion in Thio-LISICON Li10SiP2S12 solid electrolyte. *Nano Energy* **2019,** *62*, 844-852.
5. Kato, Y.; Hori, S.; Saito, T.; Suzuki, K.; Hirayama, M.; Mitsui, A.; Yonemura, M.; Iba, H.; Kanno, R., High-power all-solid-state batteries using sulfide superionic conductors. *Nature Energy* **2016,** *1* (4), 1-7.
6. Liu, Z.; Fu, W.; Payzant, E. A.; Yu, X.; Wu, Z.; Dudney, N. J.; Kiggans, J.; Hong, K.; Rondinone, A. J.; Liang, C., Anomalous high ionic conductivity of nanoporous β-Li3PS4. *J. Am. Chem. Soc.* **2013,** *135* (3), 975-978.
7. Adeli, P.; Bazak, J. D.; Park, K. H.; Kochetkov, I.; Huq, A.; Goward, G. R.; Nazar, L. F., Boosting solid-state diffusivity and conductivity in lithium superionic argyrodites by halide substitution. *Angew. Chem. Int. Ed.* **2019,** *58* (26), 8681-8686.
8. Asano, T.; Sakai, A.; Ouchi, S.; Sakaida, M.; Miyazaki, A.; Hasegawa, S., Solid Halide Electrolytes with High Lithium-Ion Conductivity for Application in 4 V Class Bulk-Type All-Solid-State Batteries. *Adv. Mater.* **2018,** *30* (44), 1803075.
9. Schlem, R.; Muy, S.; Prinz, N.; Banik, A.; Shao-Horn, Y.; Zobel, M.; Zeier, W. G., Mechanochemical synthesis: a tool to tune cation site disorder and ionic transport properties of Li3MCl6 (M= Y, Er) superionic conductors. *Adv. Energy Mater.* **2020,** *10* (6), 1903719.
10. Li, X.; Liang, J.; Luo, J.; Banis, M. N.; Wang, C.; Li, W.; Deng, S.; Yu, C.; Zhao, F.; Hu, Y., Air-stable Li 3 InCl 6 electrolyte with high voltage compatibility for all-solid-state batteries. *Energy Environ. Sci.* **2019,** *12* (9), 2665-2671.
11. Liang, J.; Li, X.; Wang, S.; Adair, K. R.; Li, W.; Zhao, Y.; Wang, C.; Hu, Y.; Zhang, L.; Zhao, S., Site-Occupation-Tuned Superionic Li x ScCl3+ x Halide Solid Electrolytes for All-Solid-State Batteries. *J. Am. Chem. Soc.* **2020,** *142* (15), 7012-7022.
12. Aono, H.; Imanaka, N.; Adachi, G.-y., High Li+ conducting ceramics. *Acc. Chem. Res.* **1994,** *27*

(9), 265-270.
13. Geng, H.; Mei, A.; Lin, Y.; Nan, C., Effect of sintering atmosphere on ionic conduction and structure of Li0. 5La0. 5TiO3 solid electrolytes. *Materials Science and Engineering: B* **2009,** *164* (2), 91-95.
14. Murugan, R.; Thangadurai, V.; Weppner, W., Fast lithium ion conduction in garnet-type Li7La3Zr2O12. *Angew. Chem. Int. Ed.* **2007,** *46* (41), 7778-7781.
15. Zhao, Y.; Daemen, L. L., Superionic conductivity in lithium-rich anti-perovskites. *J. Am. Chem. Soc.* **2012,** *134* (36), 15042-15047.
16. Richards, W. D.; Miara, L. J.; Wang, Y.; Kim, J. C.; Ceder, G., Interface stability in solid-state batteries. *Chem. Mater.* **2016,** *28* (1), 266-273.